State Estimation for Pursuer Guidance using Interacting Multiple Model based Augmented Extended Kalman filter

Sudesh K Kashyap[+||], N. Shanthakumar[||], VPS Naidu[||], Girija G[||] and Raol J.R[|| $]

Multi Sensor Data Fusion Lab, Flight Mechanics and Control Division

National Aerospace Laboratories

Bangalore-560017, India

Extended Abstract (almost a draft paper)

1. Introduction

In pursuers or interceptors, active radar seeker is used to measure relative range, relative range rate, LOS angles and rates between pursuer and evader. Using these measurements which are contaminated by high degree of noise due to Glint, Radar Cross Section (RCS) fluctuation and thermal noise, the true LOS rates have to be estimated for PN (Proportional navigation) guidance of the pursuer [1]. For advanced proportional navigation (APN) guidance, target acceleration is also required. To achieve all these, an estimator or seeker filter is required which processes the seeker measurements recursively to obtain the signals required for guidance of pursuer towards evader.

The design of the estimator is complex because not only the cumulative effects of the noise are highly non-Gaussian and time correlated but there is a periodic loss of seeker measurements due to eclipsing effects. Also the seeker measurements are available in inner Gimbal frame necessitating the use of an extended Kalman filter (EKF) for the estimator. In this paper, in order to handle the non Gaussian noise, an augmented EKF (AEKF) has been evolved using the models of RCS and glint noise effects as additional states.

In any pursuer-evader engagement, the evader would execute maneuvers to avoid the pursuer. In order to track these maneuvering targets, Interacting multiple model or IMM [2] is generally used. IMM is essentially an adaptive estimator which is based on assumption that a finite number of models are required to characterize the target at all times and which takes care of model switching implicitly. In this paper, for pursuer-evader engagement applications, the IMM based on the soft switching between a set of pre-defined target models such as constant velocity, constant acceleration, constant jerk [3] has been implemented.

[||] Scientists, [$] Head of Flight Mechanics and Control Division
+Corresponding Author's E-mail: **sudesh@css.nal.res.in**

At each instant of time, mode probability is calculated for each model using residual vector and innovation covariance matrix. Each of the mode matched filters used in IMM in this paper are based on the AEKF. It is expected that the estimator operating in closed loop for pursuer guidance applications, will produce low miss distances in any engagement scenario [4]. This could be achieved if the estimator produces estimates of LOS rates which have well attenuated noise characteristics with minimum lag.

This paper presents the development and performance evaluation of an IMM based AEKF in closed-loop using simulated data of typical pursuer-evader engagement scenarios. The key contribution of this paper is the introduction of augmented states to handle glint noise and RCS fluctuation in an IMM framework. Also, the estimator provides an estimate of the target acceleration that could be used for Augmented Proportional Navigation based pursuer guidance. The performance of novel algorithm is evaluated in terms of estimated states compared with true ones, residuals w.r.t. theoretical bounds, attenuation factor, miss distance and time to intercept.

2. IMM-AEKF algorithm formulation

The algorithm IMM-AEKF has been realized in MATLAB® environment. The state vector of respective mode matched filter is augmented with additional states for handling glint noise and RCS fluctuation present in measurement data. The state and measurement models used in 3 model IMM-AEKF are as follows:

2.1 State model

The state vector consists following 18 states including 6 states pertaining to glint noise and RCS fluctuations.

State vector:

$$\begin{bmatrix} \Delta x & \Delta V_x & a_{tx} & j_{tx} & \Delta y & \Delta V_y & a_{ty} & j_{ty} & \Delta z & \Delta V_z & a_{tz} & j_{tz} & \textit{gl int/ rcs states} \end{bmatrix}^T$$

The models pertaining to glint and RCS can be found in [5] and will be given in the final version of the paper.

Model 1: Constant Velocity (CV) Model

$$\begin{aligned} \Delta\dot{x} &= \Delta V_x; & \Delta\dot{V}_x &= 0; & \dot{a}_{tx} &= 0; & \dot{j}_{tx} &= 0; \\ \Delta\dot{y} &= \Delta V_y; & \Delta\dot{V}_y &= 0; & \dot{a}_{ty} &= 0; & \dot{j}_{ty} &= 0; \\ \Delta\dot{z} &= \Delta V_z; & \Delta\dot{V}_z &= 0; & \dot{a}_{tz} &= 0; & \dot{j}_{jz} &= 0; \end{aligned} \qquad (1)$$

Model 2: Constant Acceleration (CA) Model

$$\begin{aligned}
&\dot{\Delta x} = \Delta V_x; \quad \dot{\Delta V_x} = a_{tx} - a_{mx}; \quad \dot{a}_{tx} = -\left(\frac{a_{tx}}{\tau_x}\right); \quad \dot{j}_{tx} = 0; \\
&\dot{\Delta y} = \Delta V_y; \quad \dot{\Delta V_y} = a_{ty} - a_{my}; \quad \dot{a}_{ty} = -\left(\frac{a_{ty}}{\tau_y}\right); \quad \dot{j}_{ty} = 0; \\
&\dot{\Delta z} = \Delta V_z; \quad \dot{\Delta V_z} = a_{tz} - a_{mz}; \quad \dot{a}_{tz} = -\left(\frac{a_{tz}}{\tau_z}\right); \quad \dot{j}_{jz} = 0;
\end{aligned} \tag{2}$$

Model 3: Constant Jerk (CJ) Model

$$\begin{aligned}
&\dot{\Delta x} = \Delta V_x; \quad \dot{\Delta V_x} = a_{tx} - a_{mx}; \quad \dot{a}_{tx} = j_{tx}; \quad \dot{j}_{tx} = -\left(\frac{j_{tx}}{\tau_x}\right); \\
&\dot{\Delta y} = \Delta V_y; \quad \dot{\Delta V_y} = a_{ty} - a_{my}; \quad \dot{a}_{ty} = j_{ty}; \quad \dot{j}_{ty} = -\left(\frac{j_{ty}}{\tau_y}\right); \\
&\dot{\Delta z} = \Delta V_z; \quad \dot{\Delta V_z} = a_{tz} - a_{mz}; \quad \dot{a}_{tz} = j_{tz}; \quad \dot{j}_{jz} = -\left(\frac{j_{tz}}{\tau_z}\right);
\end{aligned} \tag{3}$$

where, $\Delta x, \Delta y, \Delta z$ are the relative positions and $\Delta V_X, \Delta V_Y, \Delta V_Z$ are the relative velocities of target w.r.t. missile, a_{tx}, a_{ty}, a_{tz} are the target accelerations, j_{tx}, j_{ty}, j_{tz} are the target jerks, a_{mx}, a_{my}, a_{mz} are the missile accelerations, and τ_x, τ_y, τ_z are the correlation time constants.

2.2 Measurement model

Measurement vector consists of $\begin{bmatrix} \rho & \dot{\rho} & \phi_y & \phi_z & \dot{\phi}_y & \dot{\phi}_z \end{bmatrix}^T$ during non-eclipsing period and $\begin{bmatrix} \rho & \dot{\rho} & \phi_y & \phi_z \end{bmatrix}^T$ during eclipsing period

where, ρ is range-to-go,

$\dot{\rho}$ is range rate,

ϕ_y and ϕ_z are Gimbal angles in yaw and pitch planes respectively,

$\dot{\phi}_y$ and $\dot{\phi}_z$ are the respective LOS rates in inner Gimbal frame.

The relative position and velocity states of the target w.r.t missile in inertial frame is transformed to LOS frame using:

$$\rho = \sqrt{\Delta x^2 + \Delta y^2 + \Delta z^2} \quad ; \quad \dot{\rho} = \frac{\Delta x \Delta \dot{x} + \Delta y \Delta \dot{y} + \Delta z \Delta \dot{z}}{\rho}$$

$$\lambda_e = tan^{-1}\left(\frac{\Delta z}{\sqrt{\Delta x^2 + \Delta y^2}} \right) \; ; \quad \dot{\lambda}_e = \frac{\Delta \dot{z}\left(\Delta x^2 + \Delta y^2 \right) - \Delta z \left(\Delta x \Delta \dot{x} + \Delta y \Delta \dot{y} \right)}{\rho^2 \sqrt{\Delta x^2 + \Delta y^2}} \tag{4}$$

$$\lambda_a = tan^{-1}\left(\frac{\Delta y}{\Delta x} \right) \quad ; \quad \dot{\lambda}_a = \frac{\left(\Delta x \Delta \dot{y} - \Delta y \Delta \dot{x} \right)}{\sqrt{\Delta x^2 + \Delta y^2}}$$

The measurement model during non-eclipsing period is:

$$\begin{bmatrix} \rho \\ \dot{\rho} \end{bmatrix}_m = \begin{bmatrix} \rho \\ \dot{\rho} \end{bmatrix}$$

$$\begin{bmatrix} \phi_y \\ \phi_z \end{bmatrix}_m = \begin{bmatrix} \phi_y \\ \phi_z \end{bmatrix}$$

$$\begin{bmatrix} 0 \\ \dot{\phi}_y \\ \dot{\phi}_z \end{bmatrix}_m = C_f^g \, C_b^f \, C_i^b \, C_l^i \begin{bmatrix} -\dot{\lambda}_a \sin \lambda_e \\ \dot{\lambda}_e \\ \dot{\lambda}_a \cos \lambda_e \end{bmatrix} \tag{5}$$

The measurement model during eclipsing period is:

$$\begin{bmatrix} \rho \\ \dot{\rho} \end{bmatrix}_m = \begin{bmatrix} \rho \\ \dot{\rho} \end{bmatrix}$$

$$\begin{bmatrix} \phi_y \\ \phi_z \end{bmatrix}_m = \begin{bmatrix} \phi_y \\ \phi_z \end{bmatrix} \tag{6}$$

where

$$\phi_y = tan^{-1}\left(\frac{m}{l} \right)$$

$$\phi_z = tan^{-1}\left(\frac{n}{\sqrt{l^2 + m^2}} \right) \quad \text{and} \quad \begin{bmatrix} l \\ m \\ n \end{bmatrix} = C_b^f C_i^b C_l^i \begin{bmatrix} 1 \\ 0 \\ 0 \end{bmatrix} \tag{7}$$

DCM for LOS to inertial frame transformation is:

$$C_l^i = \begin{bmatrix} \cos \lambda_e \cos \lambda_a & -\sin \lambda_a & -\sin \lambda_e \cos \lambda_a \\ \cos \lambda_e \sin \lambda_a & \cos \lambda_a & -\sin \lambda_e \sin \lambda_a \\ \sin \lambda_e & 0 & \cos \lambda_e \end{bmatrix} \tag{8}$$

DCM for inertial to body frame transformation is:

$$C_i^b = \begin{bmatrix} q_4^2 + q_1^2 - q_2^2 - q_3^2 & 2(q_1 q_2 + q_3 q_4) & 2(q_1 q_3 - q_2 q_4) \\ 2(q_1 q_2 - q_3 q_4) & q_4^2 - q_1^2 + q_2^2 - q_3^2 & 2(q_2 q_3 + q_1 q_4) \\ 2(q_1 q_3 + q_2 q_4) & 2(q_2 q_3 - q_1 q_4) & q_4^2 - q_1^2 - q_2^2 + q_3^2 \end{bmatrix} \quad (9)$$

where, q_1, q_2, q_3, q_4 are the attitude quaternion of the missile

DCM for body to fin frame transformation is:

$$C_b^f = \begin{bmatrix} 1 & 0 & 0 \\ 0 & \frac{1}{\sqrt{2}} & \frac{1}{\sqrt{2}} \\ 0 & -\frac{1}{\sqrt{2}} & \frac{1}{\sqrt{2}} \end{bmatrix} \quad (10)$$

DCM for fin to inner Gimbal frame transformation is:

$$C_f^g = \begin{bmatrix} \cos\phi_z \cos\phi_y & \cos\phi_z \sin\phi_y & \sin\phi_z \\ -\sin\phi_y & \cos\phi_z & 0 \\ -\sin\phi_z \cos\phi_y & -\sin\phi_z \sin\phi_y & \cos\phi_z \end{bmatrix} \quad (11)$$

3. Pursuer-evader engagement simulation

The close-loop simulation is carried to emulate a typical pursuer-evader terminal phase scenario. In order to do so, a typical 6DOF missile dynamics has been simulated and relative measurements containing target information are generated in inner-Gimbal frame in terms of range, range rate, 2 Gimbal angles and 2 LOS rates in Pitch and Yaw planes. During terminal guidance, at every sampling time measurement noise is added to true $(r, \dot{r}, \phi_g, \gamma_g, \dot{\phi}_g, \dot{\gamma}_g)$ to generate the measurements. Gaussian noise is added to the range and range rate measurements, random colored noise with bore sight error is added to Gimbal angle measurements and thermal Gaussian, correlated glint and RCS fluctuation noise are added to the LOS rate measurements. Further, data loss in LOS rates due to PRF and closing velocity has also been simulated. The data is sampled at 0.01 secs. In addition, the LOS rates also have the component of body rates affecting it. The measured data is then processed by IMM-AEKF algorithm and guidance commands are generated and fed back to missile autopilot which in turn provides sufficient fin deflections to drive the missile towards the evader.

3.1 Evader data simulation

In order to simulate realistic missile-target engagement, the following points are considered:

- In the presence of adversary, the target generally executes a turn and accelerates at short range to go (≈ 2 km).
- Target velocity to be maintained at 300 to 400 kmph.
- Target turns (velocity vector) at the rate of 20 to 25 deg/sec.
- Target under goes maximum roll rate (≈ 270 deg/sec) to generate glint effect.

Keeping the above points in mind, the evader performing evasive maneuver is simulated within the permissible 'g' limit of a typical fighter aircraft at different altitudes as shown in Table 1. It should be noted that the target speeds are chosen to achieve the desired turn rates in the range of 20-25 d/s. T he different data sets have been generated by allowing the target to maneuver continuously with the g-values given in Table 1 once the specified R_{go} is reached.

4. Performance evaluation of IMM-AEKF in closed loop

The performance of IMM-AEKF is evaluated in a close loop simulation of missile-target engagement.

The filter initialization is done as shown below:

- initial state vector

$\Delta\hat{x} = \Delta x + 100$; $\quad \Delta\hat{\dot{x}} = \Delta\dot{x} + 20$; $\quad \hat{a}_{t_x} = 0$; $\quad \hat{j}_{t_x} = 0$;

$\Delta\hat{y} = \Delta y - 50$; $\quad \Delta\hat{\dot{y}} = \Delta\dot{y} - 5$; $\quad \hat{a}_{t_y} = 0$; $\quad \hat{j}_{t_y} = 0$;

$\Delta\hat{z} = \Delta z + 50$; $\quad \Delta\hat{\dot{z}} = \Delta\dot{z} - 5$; $\quad \hat{a}_{t_z} = 0$; $\quad \hat{j}_{t_z} = 0$;

- initial state error covariance :

$\hat{P}(0/0) = 10000 * eye(ns, ns)$

- initial process noise covariance :

CV model:

Q.v = diag[0.0 5.5555e-3 0.05 5.5555e-3 0.0 5.5555e-3 0.05 5.5555e-3
0.0 5.5555e-3 0.05 5.5555e-3 1e-3 1e-3 1e-3 1e-3 1e-3 1e-3]

CA model:

Q.a = 100*Q.v

CJ model:

Q.j = 10*Q.a

- Measurement noise covariance:

$$R = diag\begin{bmatrix} 2.5e3 & 1e2 & 7.6e-5 & 7.6e-5 & 2.467e-2 & 2.467e-2 \end{bmatrix}$$

- Initial mode probability

$$\mu = \begin{bmatrix} 0.3 & 0.3 & 0.4 \end{bmatrix}$$

- Mode transition probability

$$p = \begin{bmatrix} 0.800 & 0.100 & 0.100 \\ 0.0009 & 0.999 & 0.0001 \\ 0.0009 & 0.0001 & 0.999 \end{bmatrix}$$

The 3 model IMM-AEKF is integrated with 6 DOF missile simulation model in closed loop. In order to generate smooth target acceleration estimates for MPN guidance, innovation smoothing using a low pass filter with a cut off frequency of 3Hz is used in the IMM-AEKF filter. Table 2 shows the results of closed loop missile-target simulation for all the 12 cases listed in Table 1 in terms of miss distances and time to intercept achieved by IMM-AEKF. The miss distances achieved are within acceptable limits. To achieve lower miss distances, further tuning of the augmented model as well as the AEKF is being pursued.

Typical results for Case 1 (where maneuver is initiated at $R_{to\text{-}go}$ = 10km at an altitude of 0.5km) are given in Figs. 1-13. In figs. 1-6, the comparison of estimated, true and noisy measurement signals are shown along with the estimation errors. The estimates are close to the true values in most of the cases. Figs. 7-12 show the comparison of estimated states with true values. The comparison is fairly good except for some initial transients in ΔV_y , ΔV_z estimates. The estimation errors are well within the 1σ bounds.

The mode probabilities are shown in Figs. 13-15 for engagement at an altitude of 0.5 km and with target maneuvers initiated at $R_{to\text{-}go}$ = 10km, 5km and 2.5 km. respectively (cases 1 to

3). Since the target is in a continuous accelerating mode in all the cases, the mode probability pertaining to the CA model is high most of the times.

A comparison of target acceleration estimates for the target simulation cases 1 to 3 are shown in Figs. 16-18. There are large initial transients in the acceleration estimates which could perhaps be improved if a better initial estimate of the acceleration is available.

Comparison of noise attenuation factors in the measurements are shown in Figs. 19-21. It is seen that the noise attenuation factor computed using a sliding window of length 10 is well within the stipulated limit of 0.1 most of the times. Some points which are out of these limits especially in the rate measurements are perhaps due to eclipsing effects in the measurements.

5. Concluding Remarks

The performance of an IMM-AEKF algorithm, integrated with 6 degree of freedom missile simulation model, is evaluated in terms of miss distances and time for interception using twelve sets of simulated data at altitudes of 0.5km, 5km, 10km and 15km with target maneuvers initiated at different range to go. Based on the results, it is concluded that the filter performance is quite satisfactory. Some performance enhancement, could be achieved by the use of innovation smoother, lead-lag compensator and inclusion of body rate coupling into the augmented model for handling seeker noise.

References

1. Ananthasayanam M R, Sarkar A K, Bhattacharya A, Tiwari P, Vorha P: Nonlinear Observer State Estimation From Seeker Measurements and Seeker-Radar Measurements Fusion, Paper No AIAA-2005-6066-CP (2005).

2. Bar-Shalom Y and Chang K C: Tracking a Maneuvering Target Using Input Estimation Versus The Interacting Multiple Model Algorithm. IEEE Transactions On Aerospace And Electronic Systems, Vol. AES 26, No 2, March (1989).

3. Mehrotra K and Mahapatra P : A Jerk Model for Tracking Highly Maneuvering Targets, IEEE Transactions on Aerospace and Electronic Systems, Vol. AES-33, No. 4, pp 1094-1105, October (1997).

4. Zarchan P: Tactical and Strategic Missile Guidance. Vol. 176, Progress in Aeronautics and Astronautics, Third Edition, (1997).

5. Prashant Vora, Abhijit Bhattacharyya, M., Jyothi, P. K. Tiwari & R. N.Bhattacharjee, RF Seeker Modeling and Seeker Filter Design, National Workshop on Tactical Missile Guidance (NWTMG), DRDL, Hyderabad, India, February, 2004.

Table 1: Target trajectory simulation parameters

Case No.	Altitude (km)	Target Speed (m/s)	(kmph)	Maneuver (g's) pitch	yaw	Turn Rate (d/s)	Maneuver starts at R_{go} (km)
1	0.5	135	485	6	-6	24.6	10
2	0.5	135	485	6	-6	24.6	5
3	0.5	135	485	6	-6	24.6	2.5
4	5.0	140	500	6	-6	23.7	10
5	5.0	140	500	6	-6	23.7	5
6	5.0	140	500	6	-6	23.7	2.5
7	10.0	150	540	6	-6	22.1	10
8	10.0	150	540	6	-6	22.1	5
9	10.0	150	540	6	-6	22.1	2.5
10	15.0	150	540	6	-6	22.1	10
11	15.0	150	540	6	-6	22.1	5
12	15.0	150	540	6	-6	22.1	2.5

Table 2: Closed loop performance evaluation results

Case No.	IMM-AEKF with glint states	
	Miss Distance (m)	Time to intercept (sec)
1	5.436	15.41
2	7.717	13.36
3	7.813	12.66
4	10.758	13.36
5	14.673	11.96
6	7.843	11.55
7	6.655	11.93
8	11.046	11.14
9	7.109	10.83
10	20.507	11.61
11	9.781	10.81
12	5.246	10.54

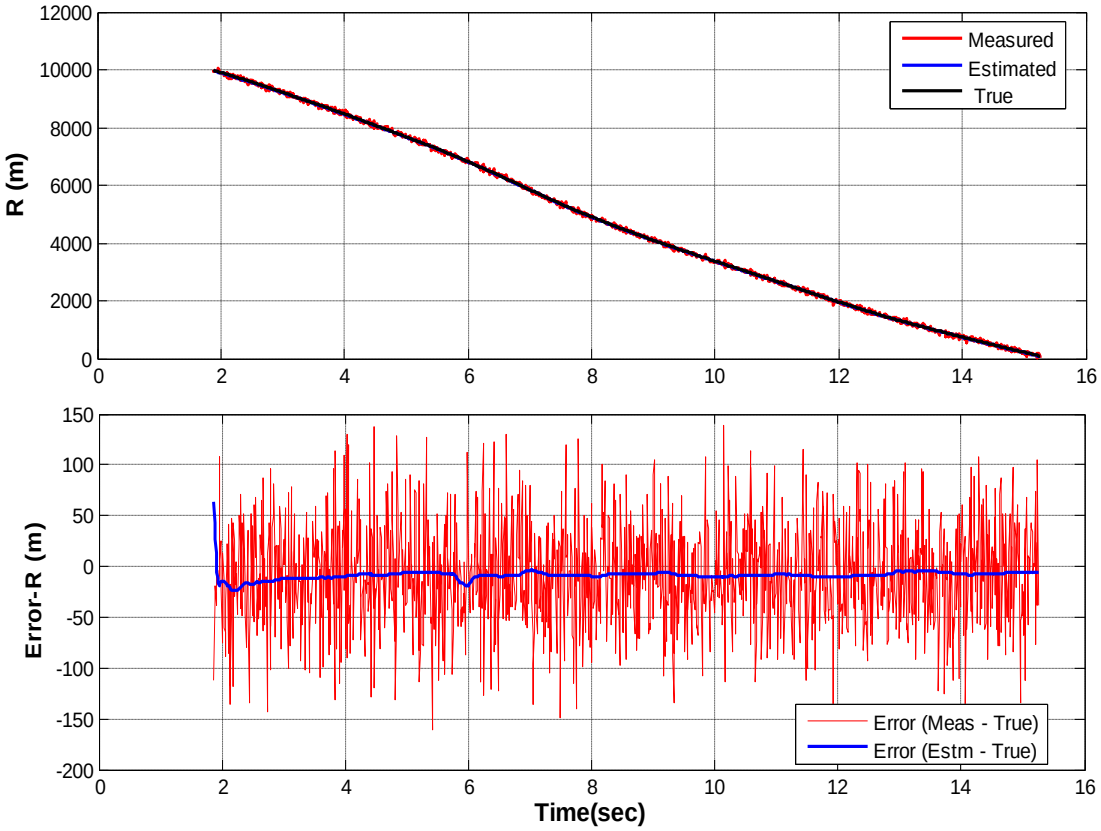

Fig. 1: Comparison of $(r_m, \hat{r}, r)$ and Estm. error (Case 1- Alt. 0.5km, man. at $R_{to\text{-}go}$=10km)

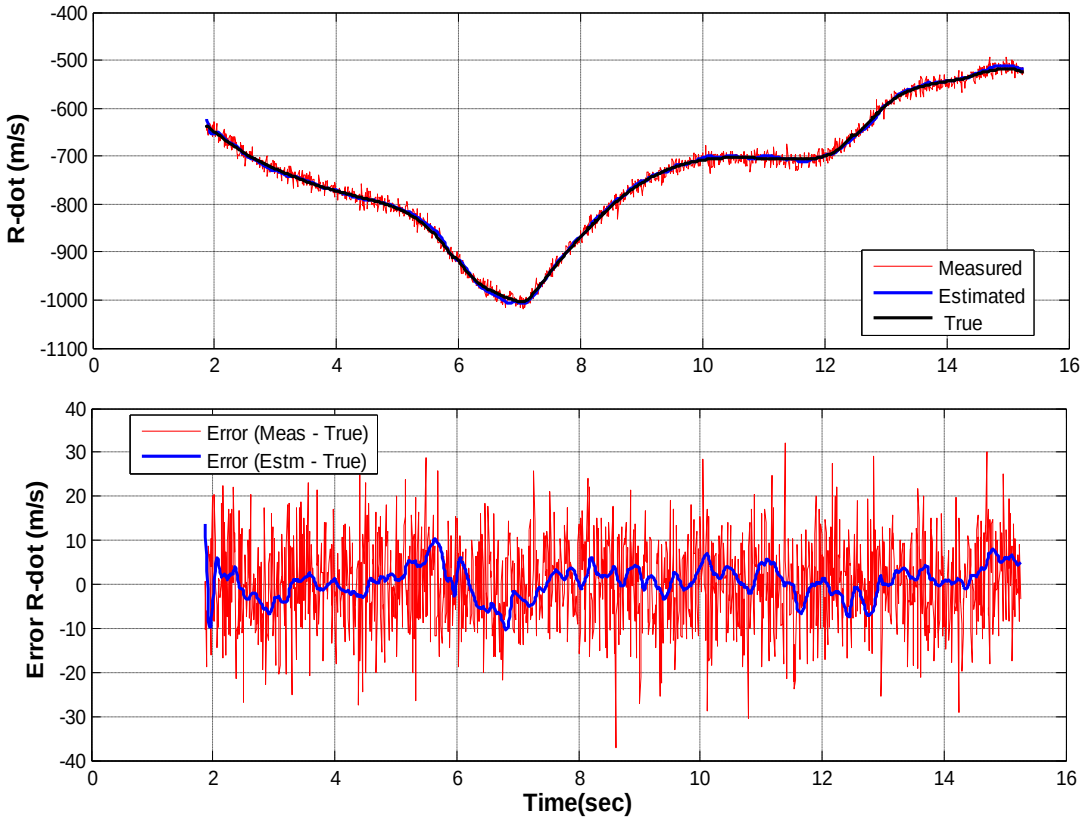

Fig. 2: Comparison of $(\dot{r}_m, \hat{\dot{r}}, \dot{r})$ and Estm. error (Case 1- Alt. 0.5km, man. at $R_{to\text{-}go}$=10km)

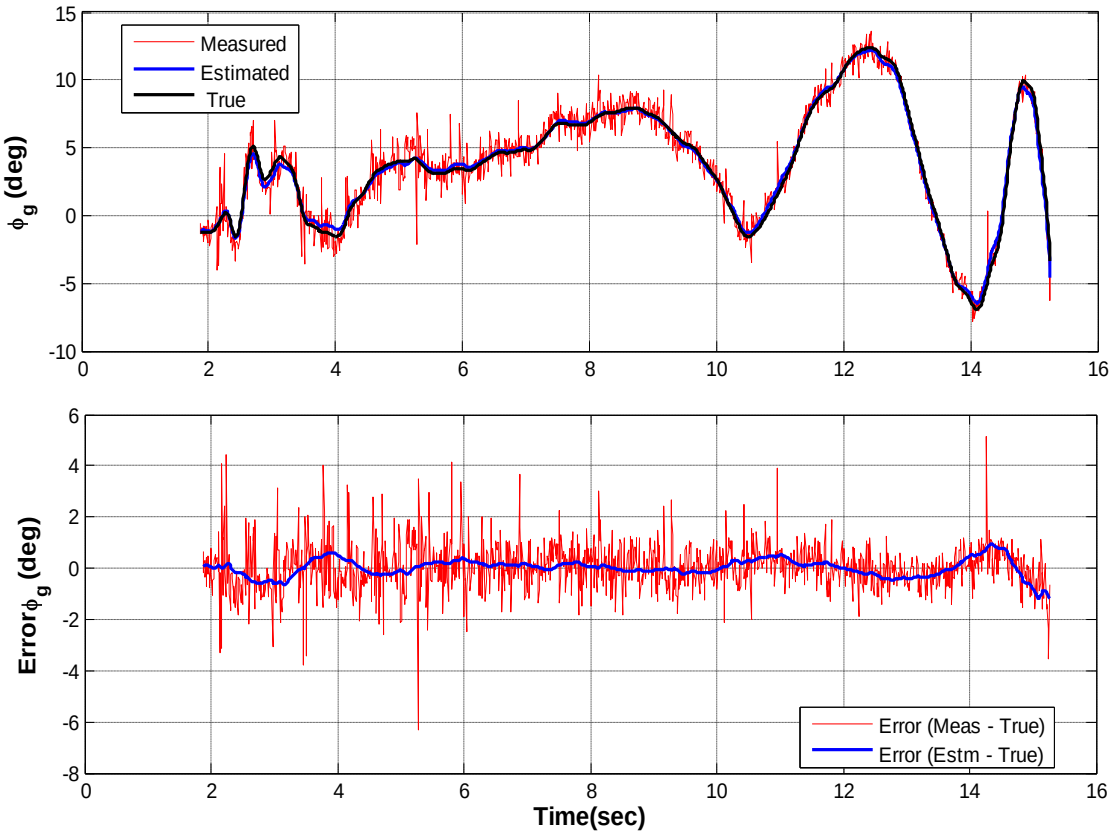

Fig. 3: Comparison of $\phi_{gm}, \hat{\phi}_g, \phi_g$ and Estm. error (Case 1- Alt. 0.5km, man. at $R_{to\text{-}go}$=10km)

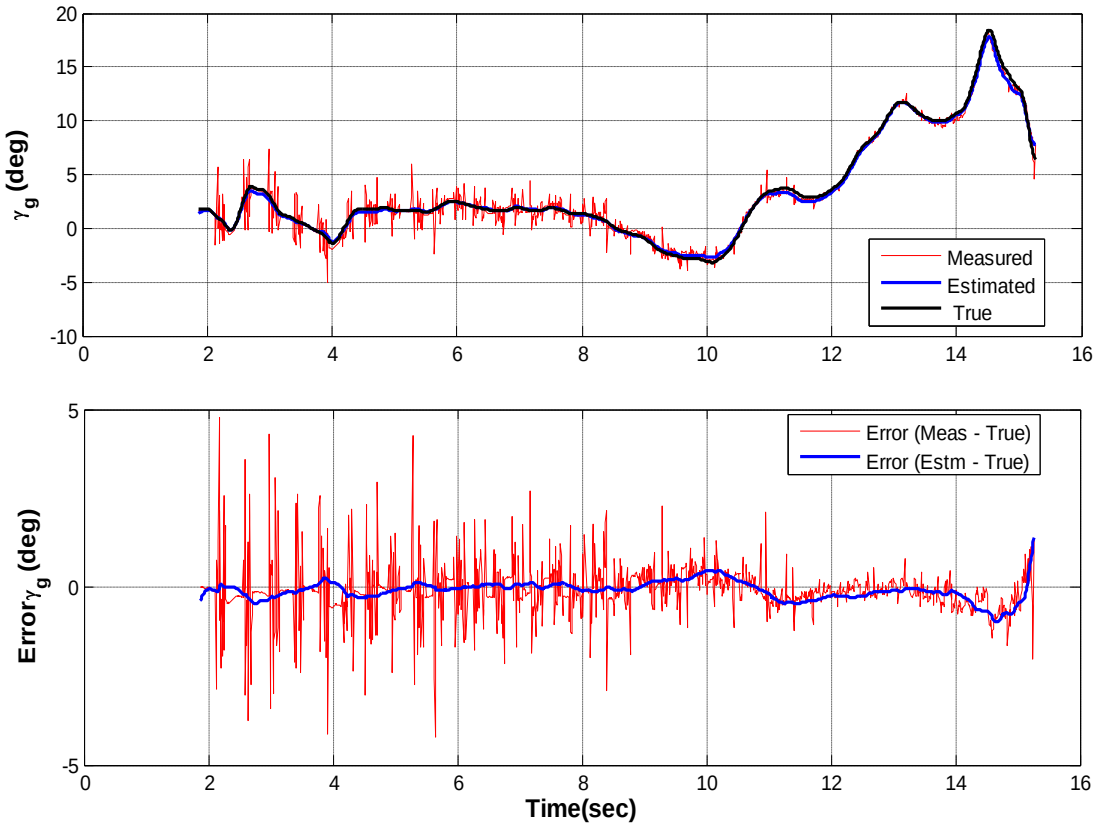

Fig. 4: Comparison of $\gamma_{gm}, \hat{\gamma}_g, \gamma_g$ and Estm. error (Case 1- Alt. 0.5km, man. at $R_{to\text{-}go}$=10km)

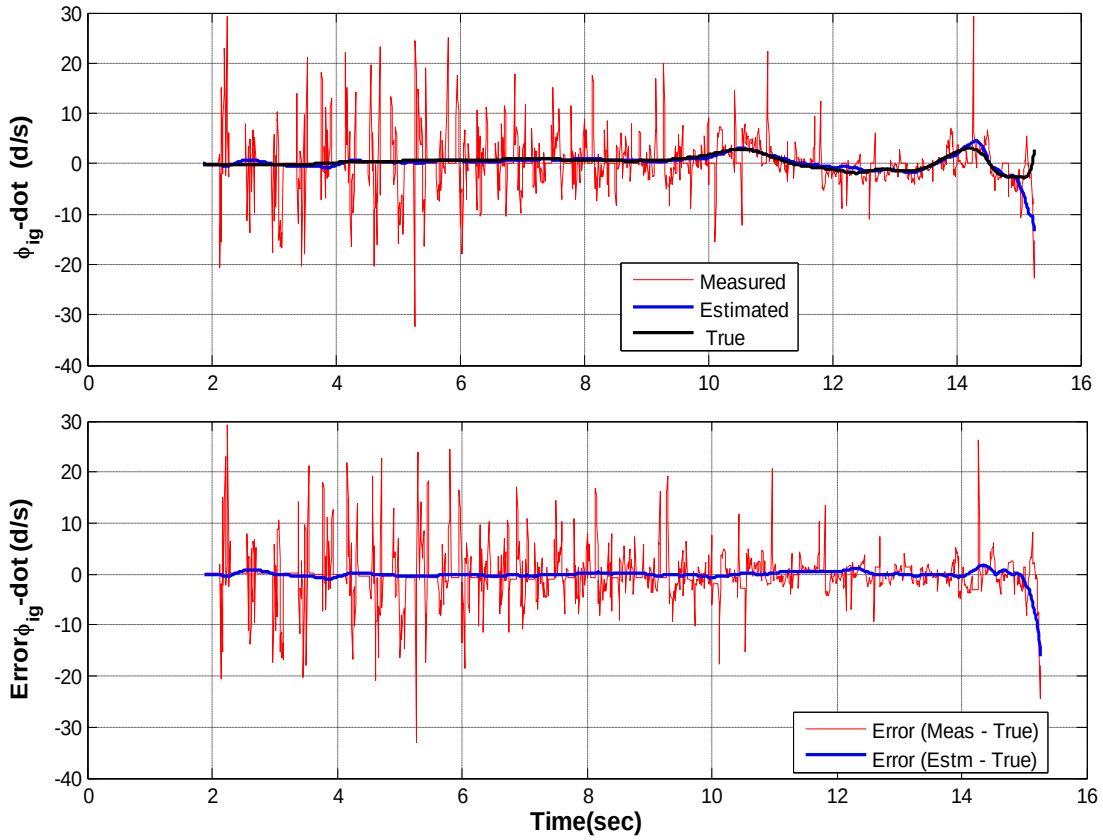

Fig. 5: Comparison of $\dot{\phi}_{gm}, \hat{\dot{\phi}}_g, \dot{\phi}_g$ and Estm. error (Case 1- Alt. 0.5km, man. at $R_{to\text{-}go}$=10km)

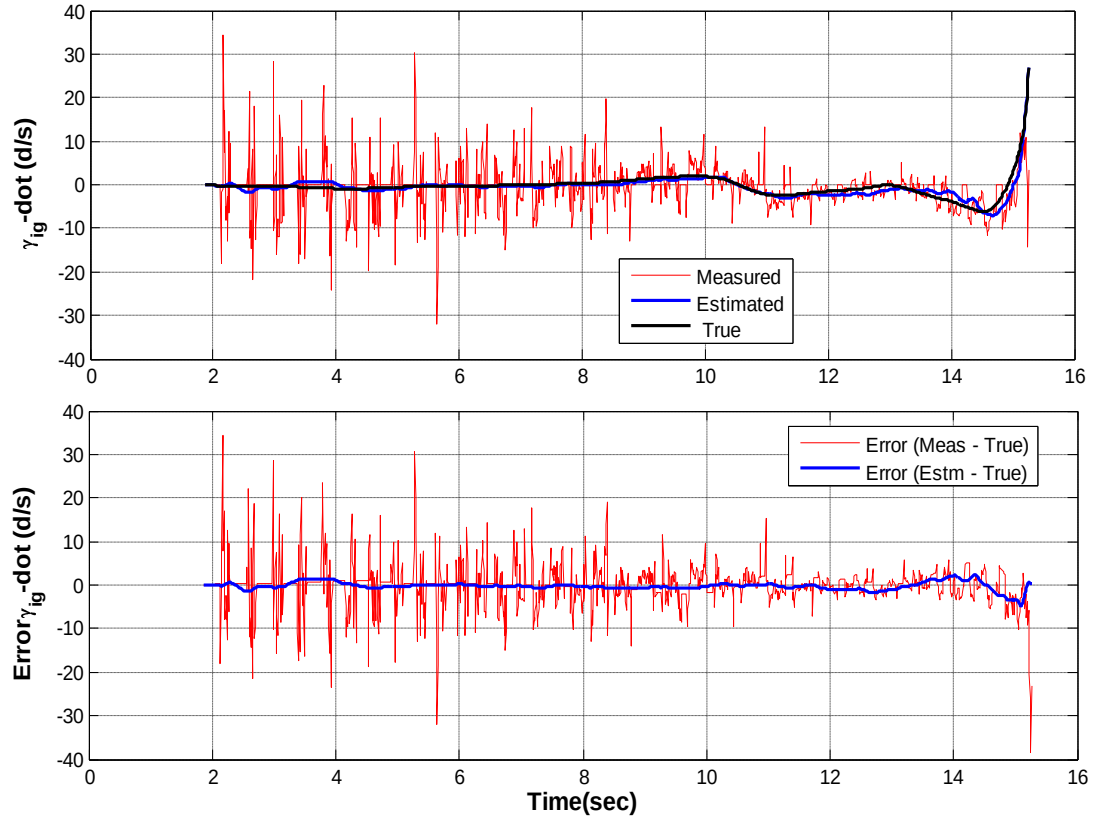

Fig. 6: Comparison of $\dot{\gamma}_{gm}, \hat{\dot{\gamma}}_g, \dot{\gamma}_g$ and Estm. error **(**Case 1- Alt. 0.5km, man. at $R_{to\text{-}go}$=10km**)**

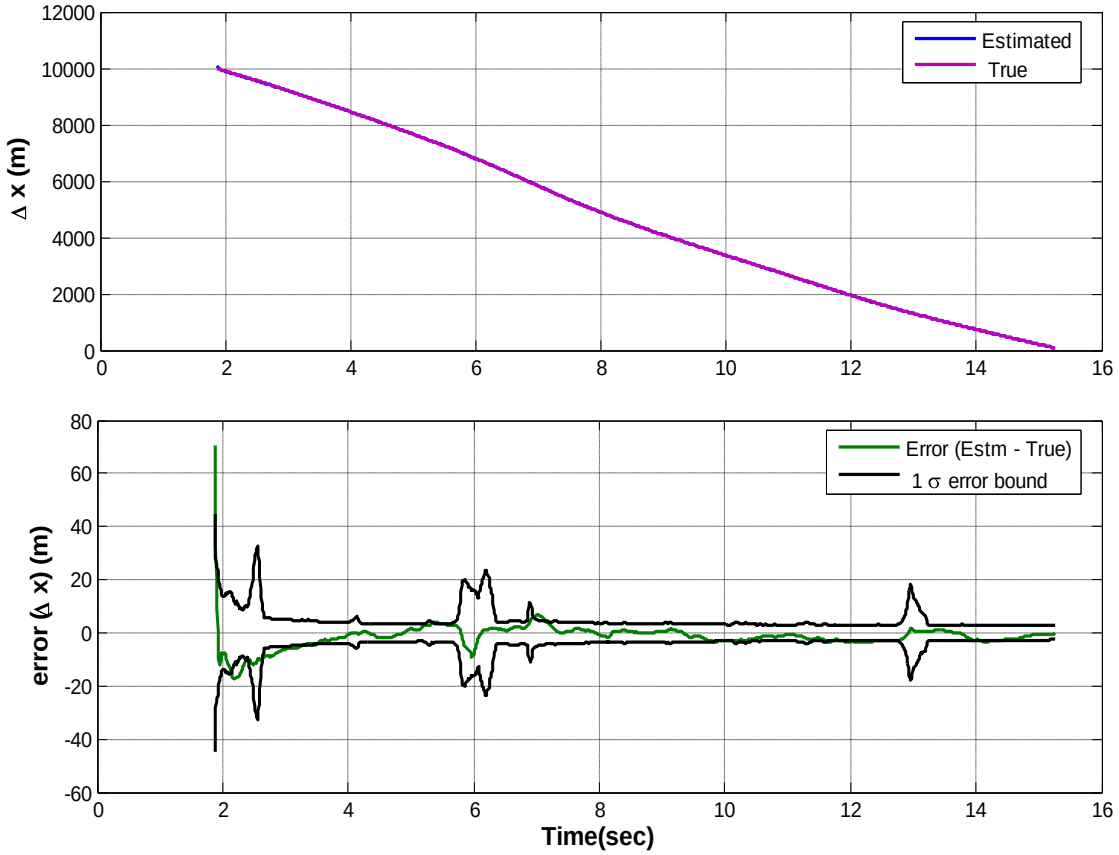

Fig. 7:Estimated states and state error with bounds (Case 1- Alt. 0.5km, man. at $R_{to\text{-}go}$=10km)

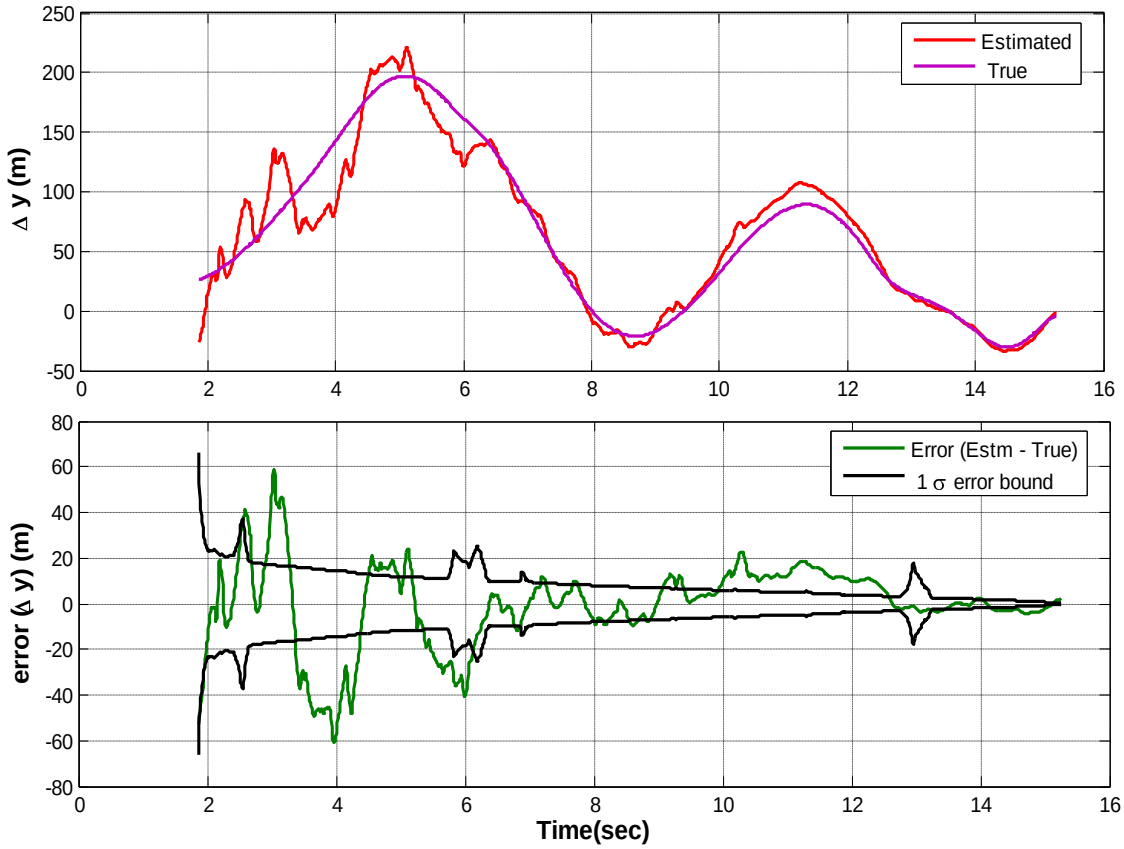

Fig. 8: Estimated states and state error with bounds (Case 1- Alt. 0.5km, man. at $R_{to\text{-}go}$=10km)

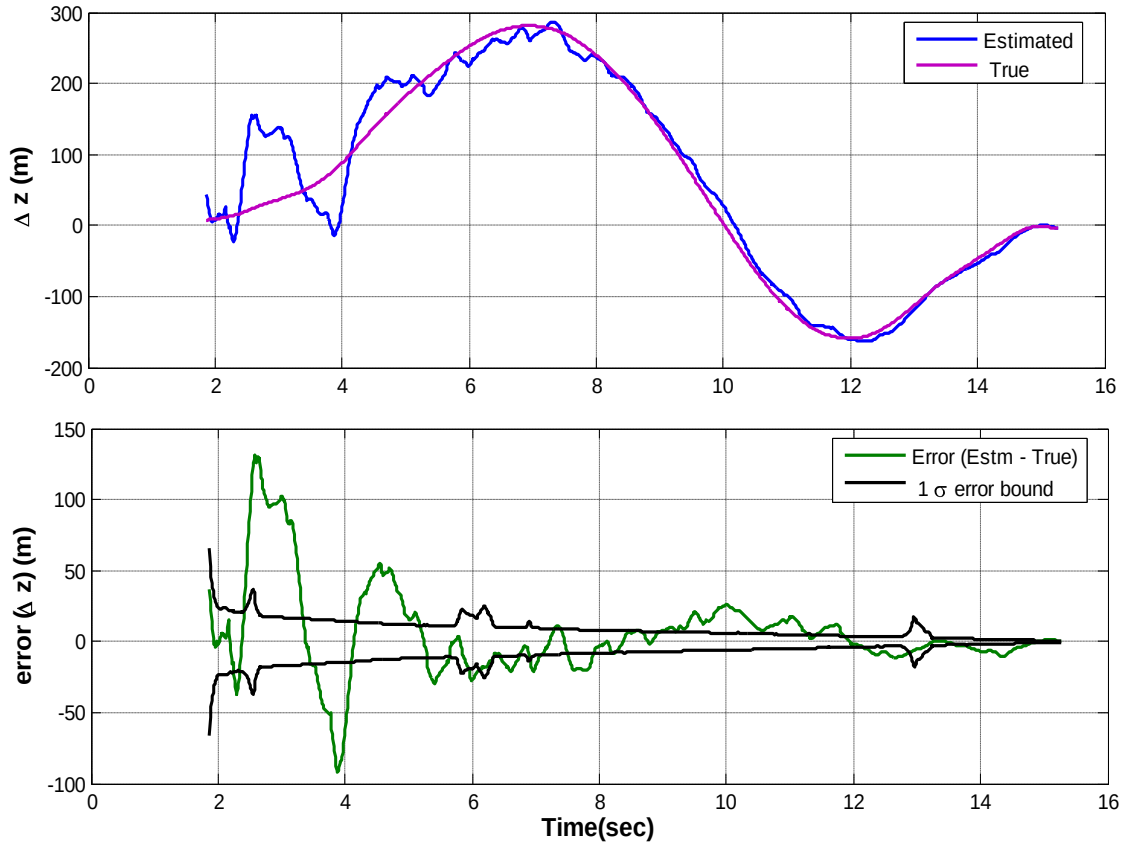

Fig. 9:Estimated states and state error with bounds (Case 1- Alt. 0.5km, man. at $R_{to\text{-}go}$=10km)

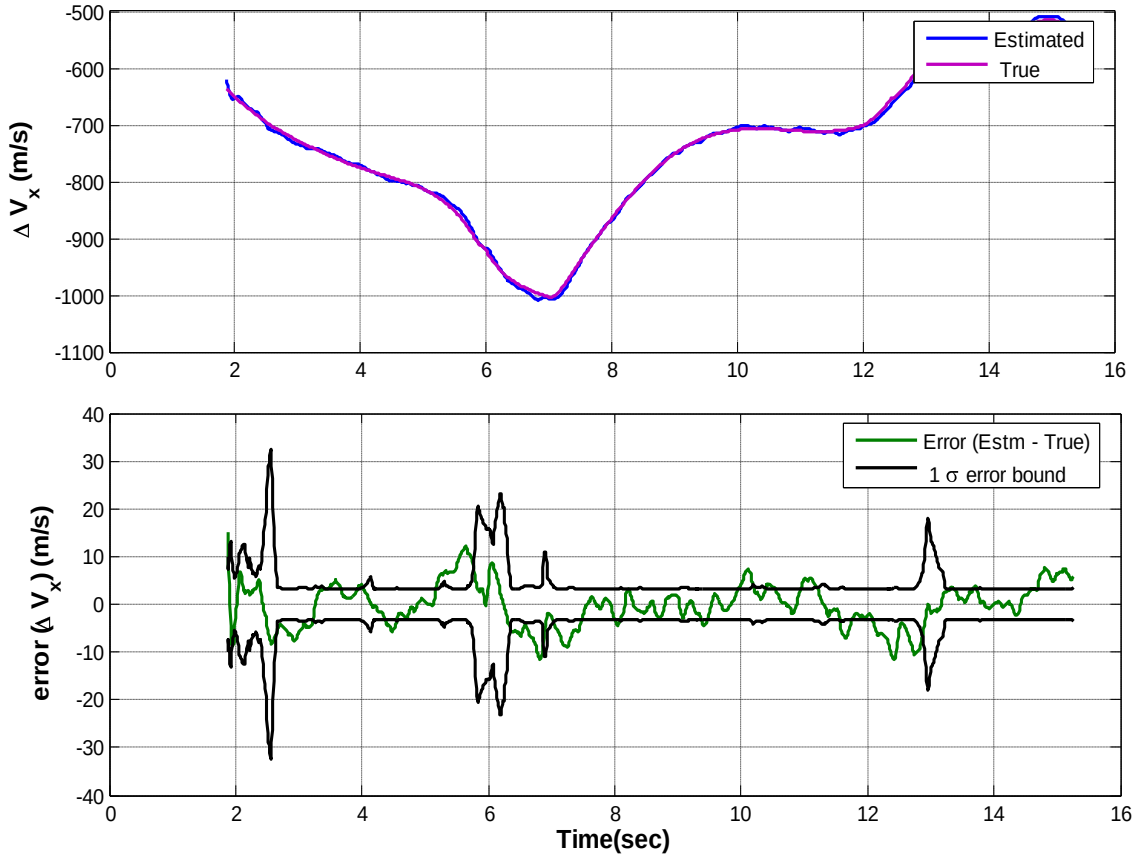

Fig. 10:Estimated states and state error with bounds (Case 1- Alt. 0.5km, man. at $R_{to\text{-}go}$=10km)

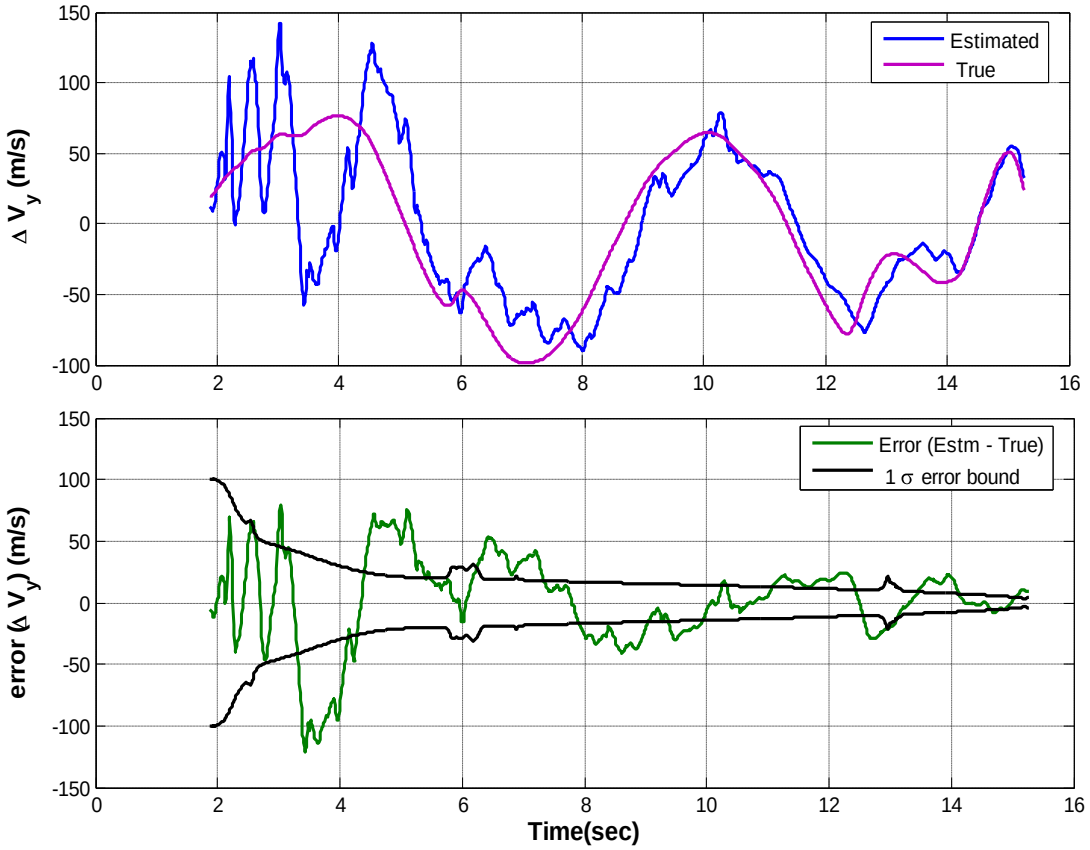

Fig. 11: Estimated states and state error with bounds (Case 1- Alt. 0.5km, man. at $R_{to\text{-}go}$=10km)

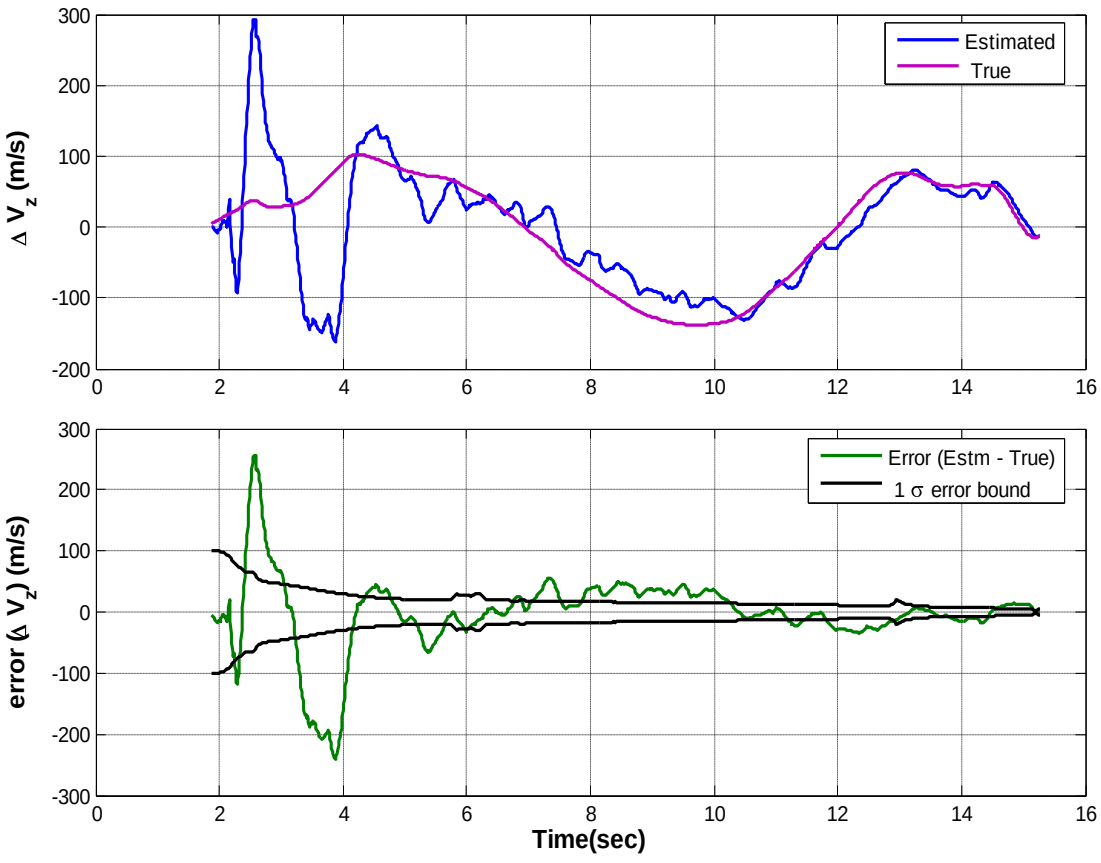

Fig. 12: Estimated states and state error with bounds (Case 1- Alt. 0.5km, man. at $R_{to\text{-}go}$=10km)

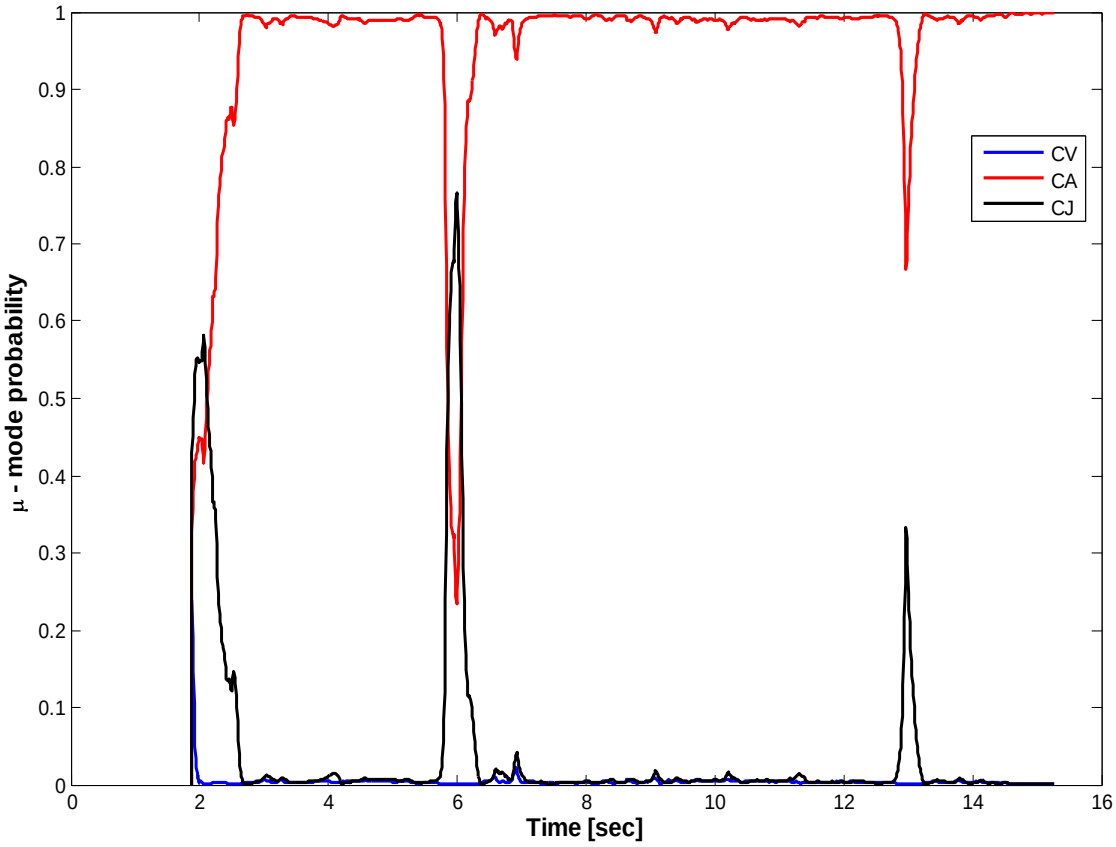

Fig. 13: Estimated Mode Probability from IMM-AEKF (Case 1- Alt. 0.5km, man. at $R_{to\text{-}go}$=10km)

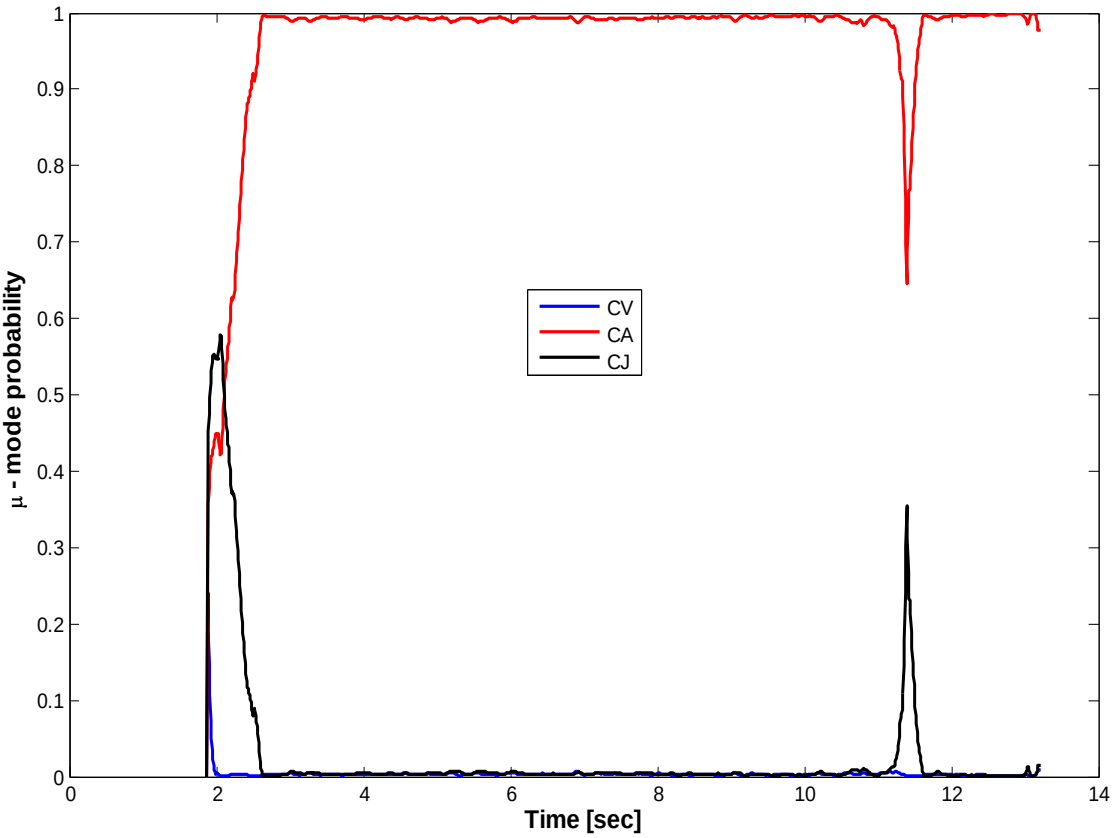

Fig. 14: Estimated Mode Probability from IMM-AEKF (Case 2- Alt. 0.5km, man. at $R_{to\text{-}go}$=5km)

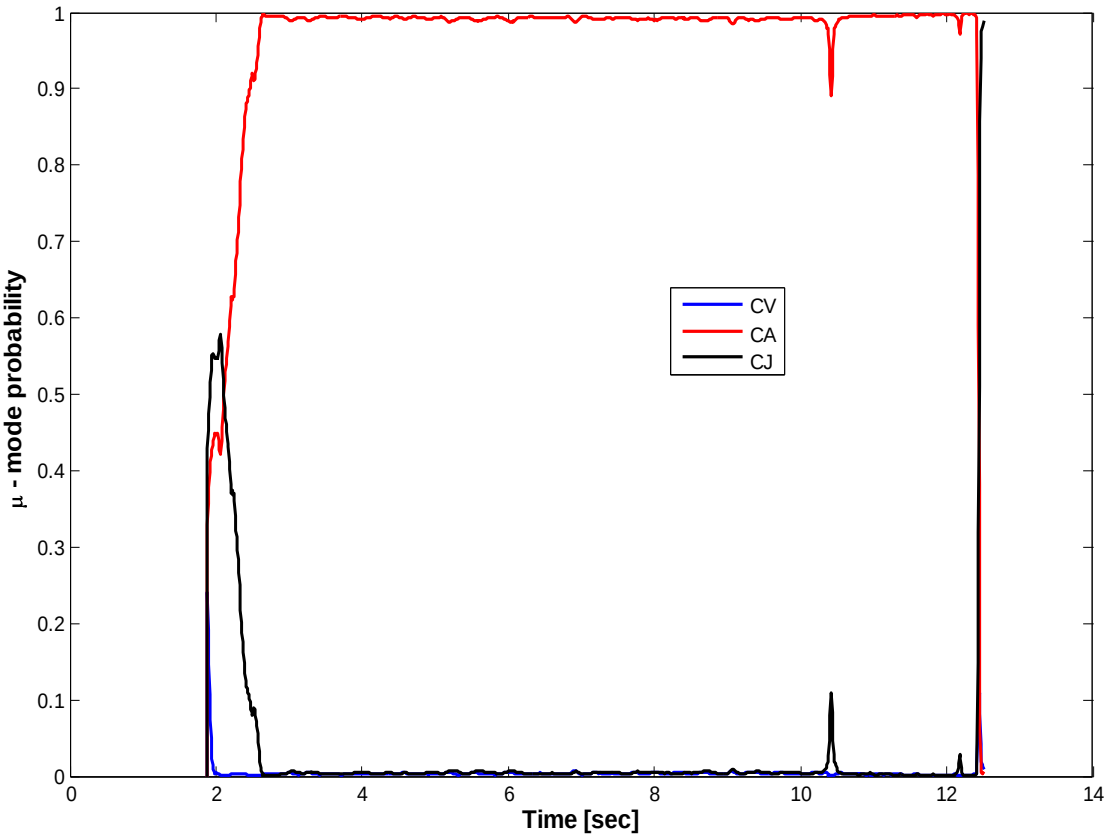

Fig. 15: Estimated Mode Probability from IMM-AEKF (Case 3- Alt. 0.5km, man. at $R_{to\text{-}go}$=2.5km)

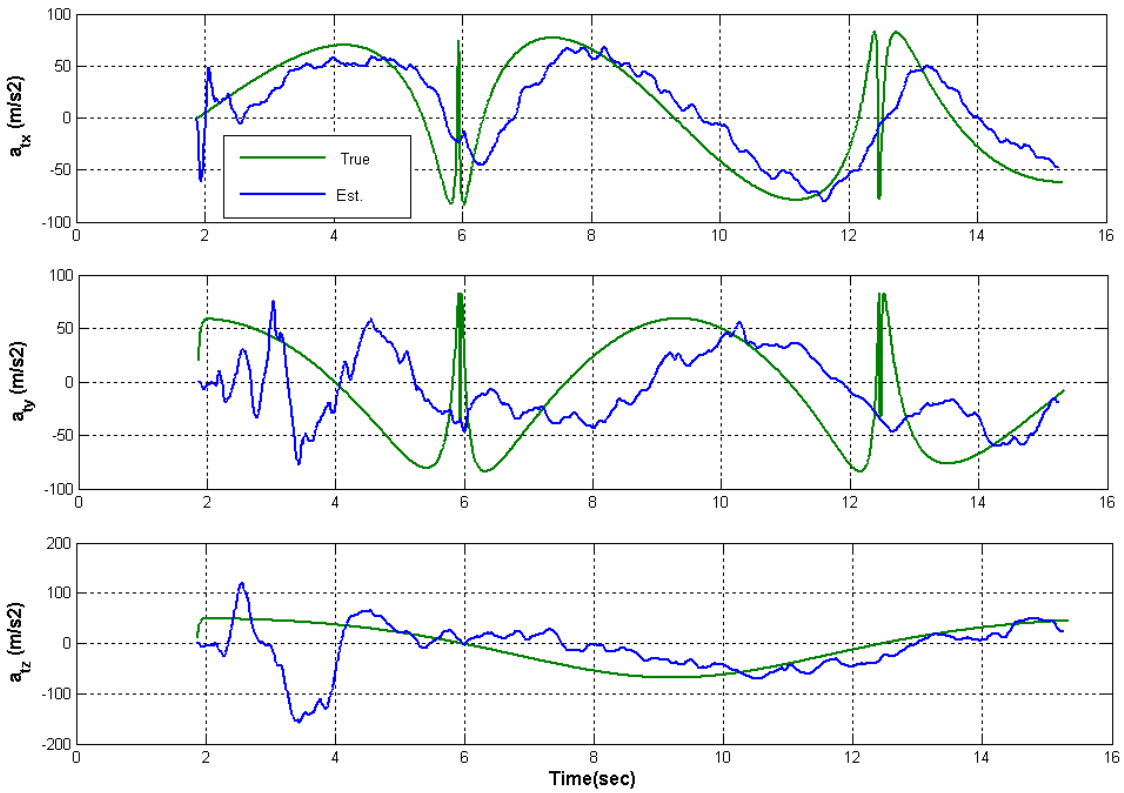

Fig. 16: Comparison of target accn. estimates (Case 1- Alt. 0.5km, man. at $R_{to\text{-}go}$=10km)

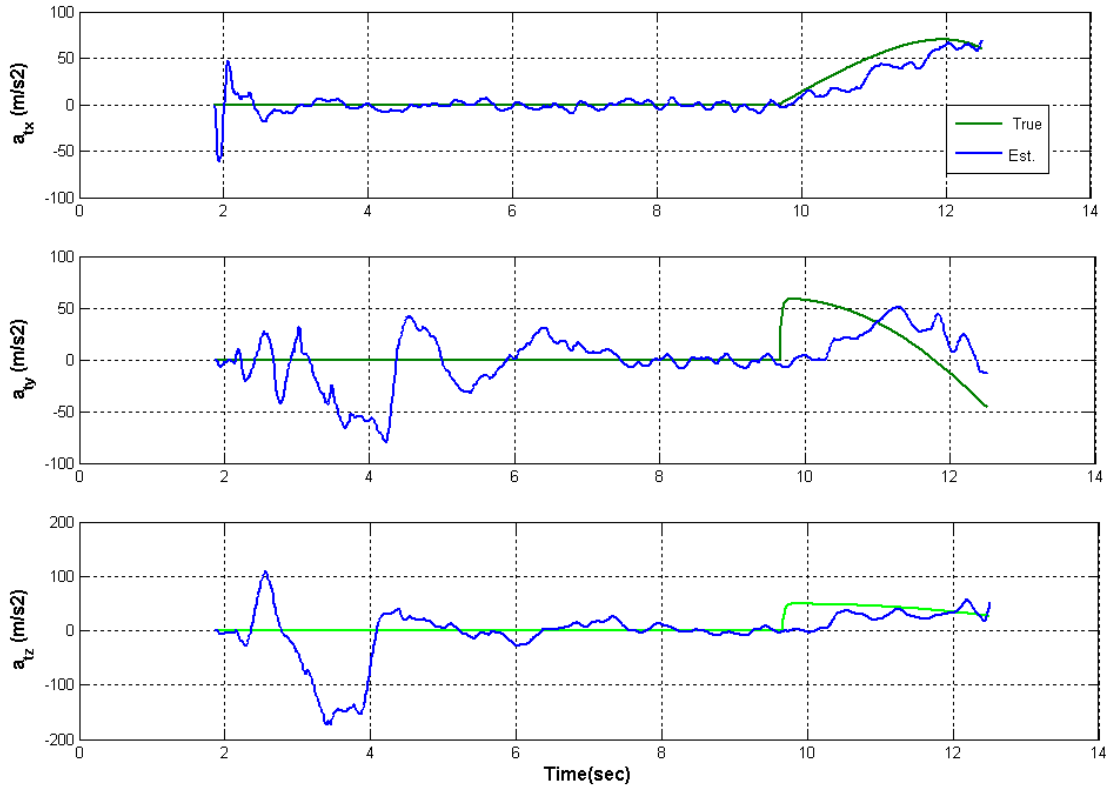

Fig. 17: Comparison of target accn. estimates (Case 2- Alt. 0.5km, man. at $R_{to\text{-}go}$=5km)

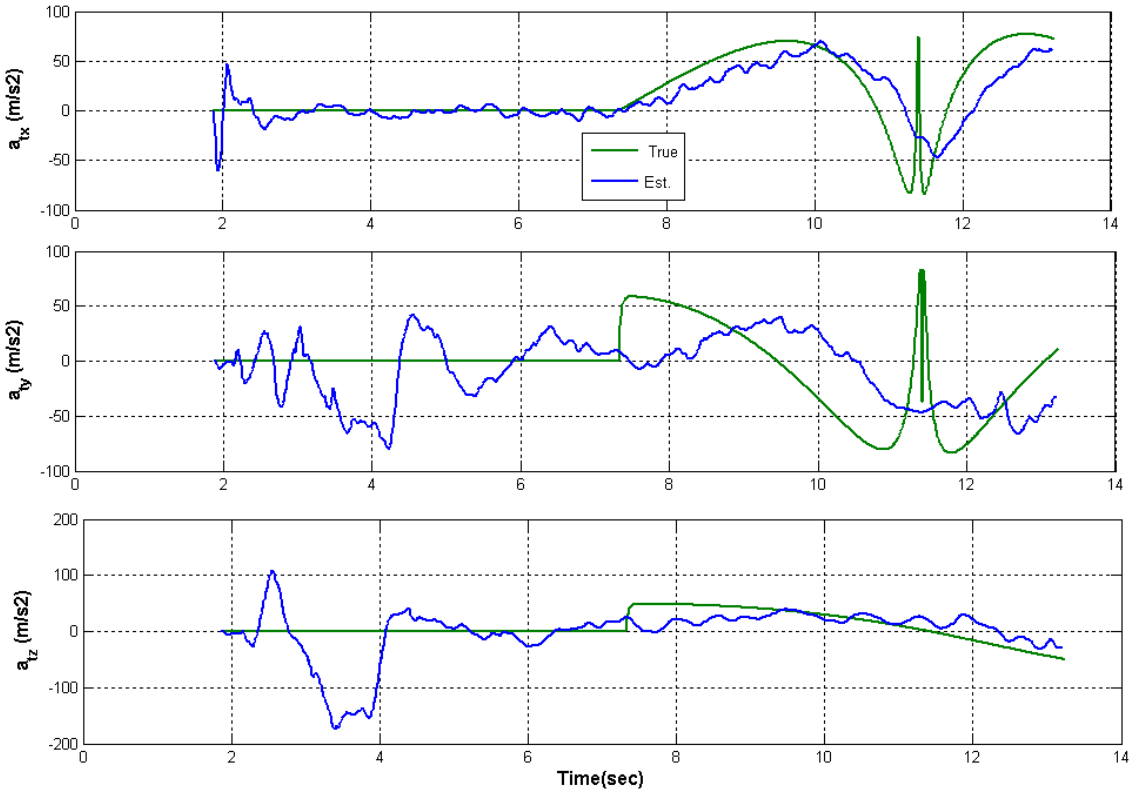

Fig. 18: Comparison of target accn. estimates (Case 1- Alt. 0.5km, man. at $R_{to\text{-}go}$=2.5km)

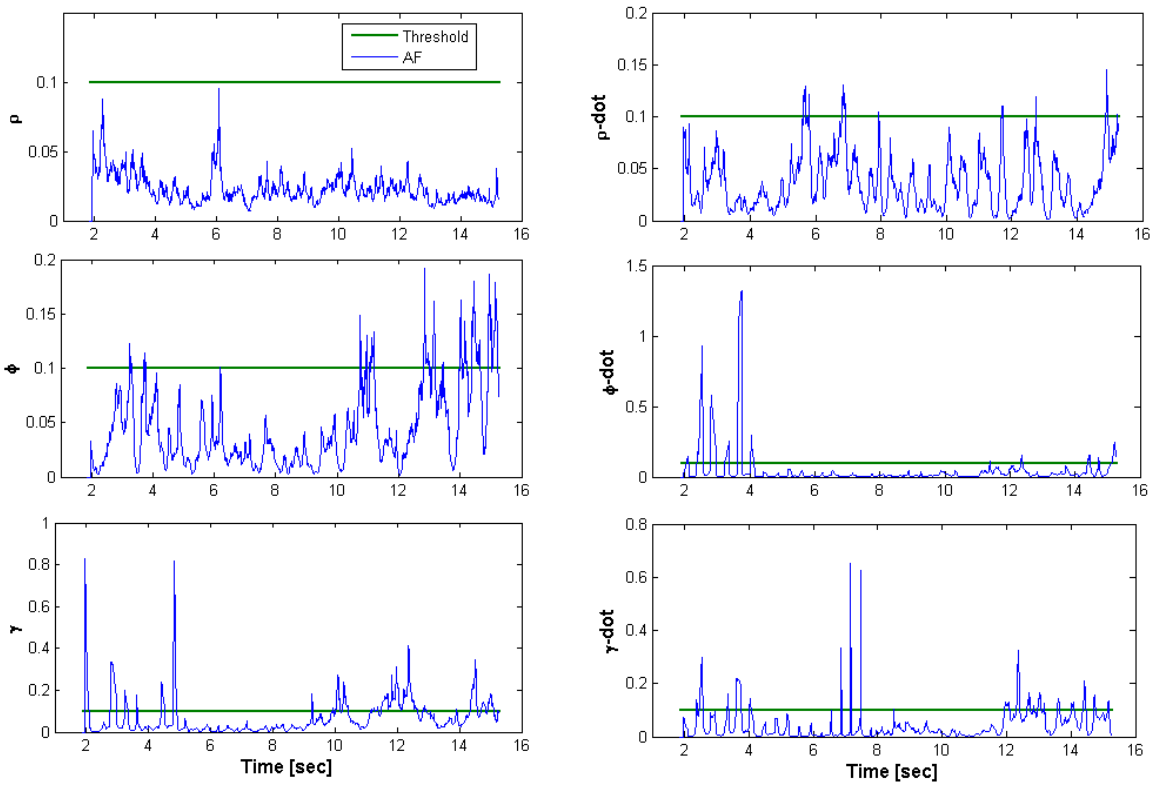

Fig. 19: Comparison of noise attenuation factors (Case 1- Alt. 0.5km, man. at $R_{to\text{-}go}$=10km)

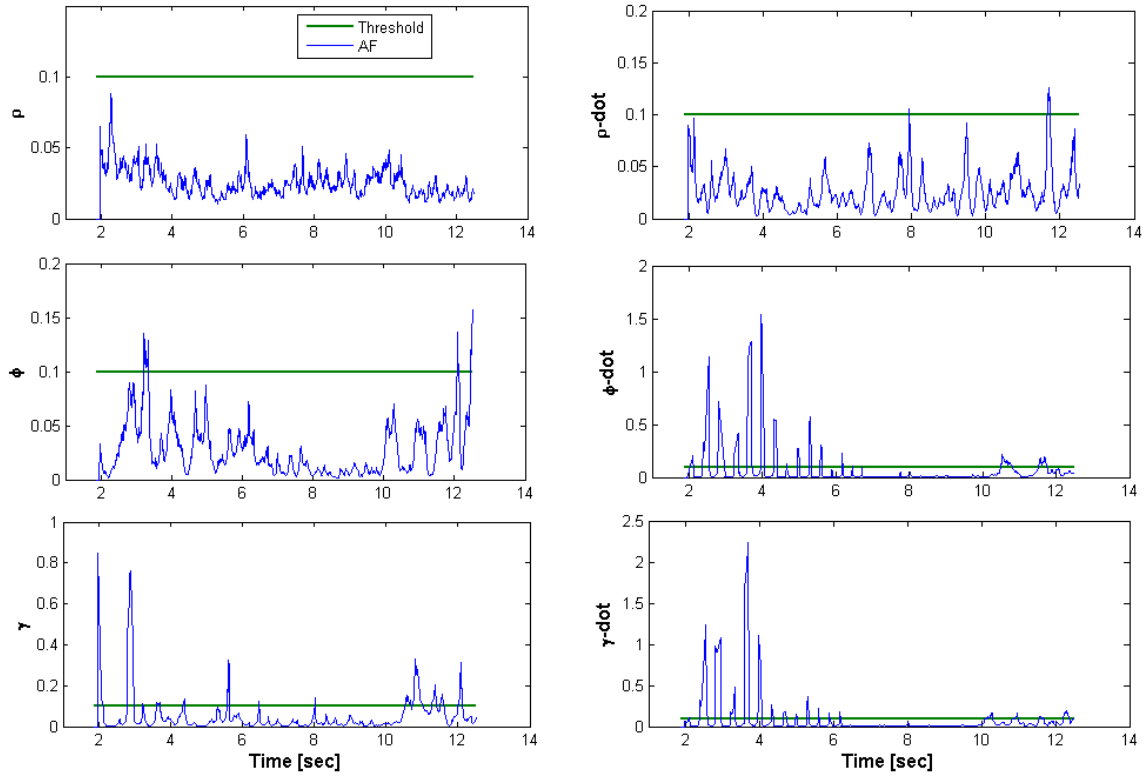

Fig. 20: Comparison of noise attenuation factor (Case 2- Alt. 0.5km, man. at $R_{to\text{-}go}$=5km)

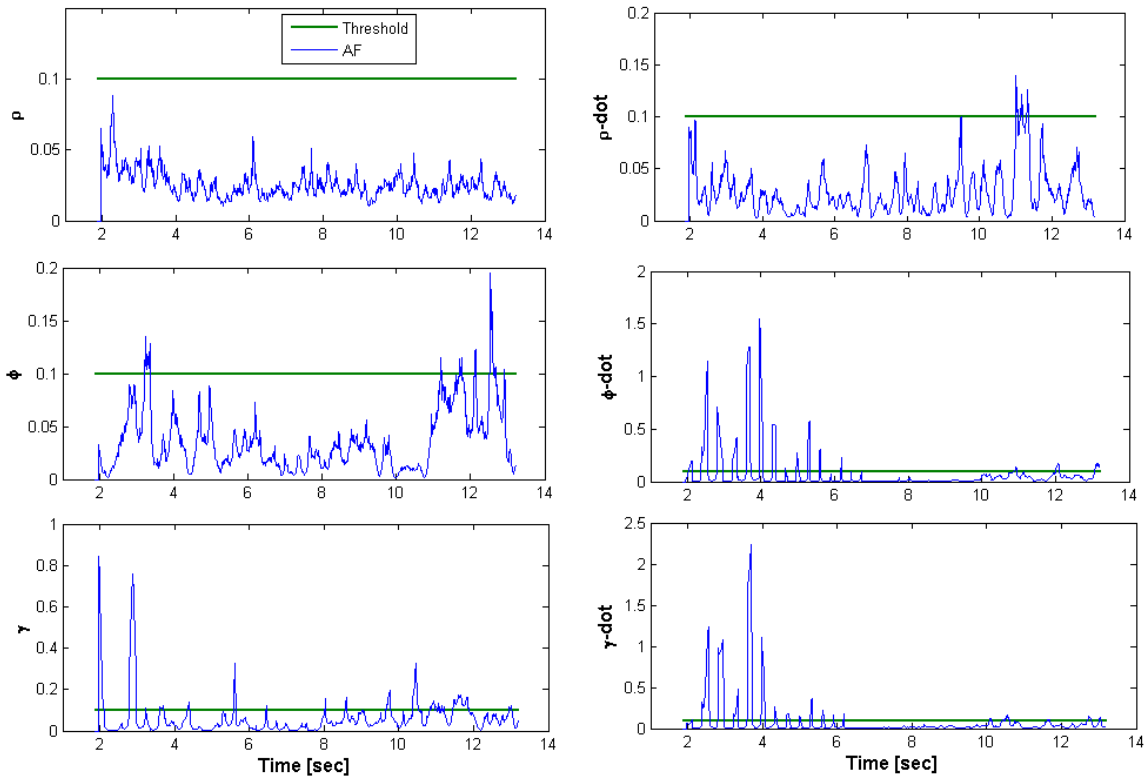

Fig. 21: Comparison of noise attenuation factor (Case 3- Alt. 0.5km, man. at $R_{to\text{-}go}$=2.5km)